

Postprint: One-Step Thermal Decomposition Fabrication of Pt Counter Electrode for Dye- Sensitized Solar Cells

Authors: Li Siqian, Huang Jie, Jian Xie, Zhang Junye, Cong Wanghao

Date: 2023-03-18T00:00:00+00:00

Abstract

Pt/FTO counter electrodes were fabricated via spin-coating and thermal decomposition of an $\text{H}_2\text{PtCl}_6 \cdot 6\text{H}_2\text{O}$ precursor solution. The effects of spin-coating/annealing cycles on the platinum loading, transmittance, and photovoltaic performance of assembled dye-sensitized solar cells (DSSCs) employing Pt/FTO counter electrodes were investigated. The results demonstrated that the cell assembled with the counter electrode prepared through 5 spin-coating/annealing cycles achieved an optimal power conversion efficiency of 6.78%, surpassing that of cells assembled with conventional magnetron sputtered counter electrodes. Based on the spin-coating cycles and Pt loading of the counter electrode under optimal photovoltaic performance conditions, the concentration and usage volume of the $\text{H}_2\text{PtCl}_6 \cdot 6\text{H}_2\text{O}$ precursor solution were further optimized. By adopting a one-step drop-coating/annealing process, Pt/FTO counter electrodes featuring high transmittance, low Pt loading, and high assembled cell efficiency were obtained. The cell assembled with the Pt/FTO counter electrode prepared by this one-step method attained a power conversion efficiency of 6.92%.

Full Text

Preamble

Vol. 29 No. 9 CHINESE JOURNAL OF MATERIALS RESEARCH
September 2015

High Efficient Pt Counter Electrode Prepared by One-step Thermal
Decomposition for Dye-sensitized Solar Cell

LI Siqian, HUANG Jie, XIE Jian, ZHANG Jun, YE Cong**, WANG Hao

(Hubei Collaborative Innovation Center for Advanced Organic Chemical Materials, Faculty of Physics and Electronic Technology, Hubei University, Wuhan 430062, China)

*Supported by National Natural Science Foundation of China Nos. 11374090 & 51372075.

Manuscript received October 8, 2014; in revised form November 13, 2014.

**To whom correspondence should be addressed, Tel: (027)88663390,
E-mail: yecong@issp.ac.cn**

ABSTRACT

The Pt counter electrode was prepared on fluorine-doped tin oxide (FTO) glass by spin-coating and subsequent thermal decomposition of $\text{H}_2\text{PtCl}_6 \cdot 6\text{H}_2\text{O}$ precursor solution. The influence of spin coating-annealing cycles on platinum loading, light transmittance of the Pt/FTO counter electrode, and the photovoltaic performance of assembled dye-sensitized solar cells (DSSCs) was investigated. The results showed that cells assembled with counter electrodes prepared by five spin coating-annealing cycles achieved an optimal power conversion efficiency of 6.78%, which was higher than that of cells using conventional magnetron sputtered counter electrodes. Based on the optimal spin coating cycles and Pt loading for best photovoltaic performance, the concentration and volume of the $\text{H}_2\text{PtCl}_6 \cdot 6\text{H}_2\text{O}$ precursor solution were further optimized. By employing a one-step drop coating-annealing process, Pt/FTO counter electrodes with high transmittance, low Pt loading, and high cell efficiency were obtained. DSSCs assembled with these one-step prepared counter electrodes achieved a power conversion efficiency of 6.92%.

KEY WORDS synthesizing and processing technics, TiO_2 nanotube arrays, Pt counter electrode, dye-sensitized solar cell, thermal decomposition, photovoltaic performance

Dye-sensitized solar cells (DSSC) are thin-film solar cells that mimic the principle of photosynthesis. Since Grätzel first applied titanium oxide nanocrystalline porous films to DSSCs in 1991, this technology has attracted significant attention due to its low cost, simple structure and fabrication process, relatively high photoelectric conversion efficiency, and pollution-free production. In DSSCs, dye sensitizers absorb photons and transition from ground state to excited state, generating photoelectrons that rapidly inject into nanoporous semiconductor materials (such as TiO_2) and transport through the porous film to reach the counter electrode via an external circuit. Meanwhile, oxidized dyes are regenerated by I^- in the electrolyte, and the reduction product I_3^- diffuses to the counter electrode where it is reduced, completing the entire cycle. The counter electrode material collects electrons from the photoanode through the external circuit and transfers them to the electron acceptor I_3^- in the electrolyte, while also catalyzing the redox reaction rate of the I^-/I_3^- couple to improve carrier collection efficiency.

Platinum is commonly used as counter electrode material, but as a precious metal with limited reserves, researchers have attempted to replace it with cheaper alternatives such as carbon, TiC, WO_2 , and VN. However, Pt remains the most catalytically active material to date, and a certain thickness of metallic Pt can also form a mirror surface that reflects unabsorbed sunlight back for secondary utilization, thereby improving solar cell efficiency. Therefore, developing efficient, low-Pt-loading counter electrodes through simple processes is crucial for enhancing cell efficiency, reducing costs, and simplifying fabrication. Several research groups have achieved promising results using simple methods to prepare low-Pt-loading counter electrodes. Lin and He et al. prepared Pt counter electrodes by electroless deposition, achieving resistances comparable to or lower than conventional sputtered Pt electrodes ($1.92 \Omega \cdot \text{cm}^2$) with significantly reduced Pt consumption and higher catalytic activity. Bach's group prepared transparent Pt counter electrodes with low resistivity and over 80% transmittance by electrodeposition, showing great potential for flexible cells on metal substrates. Xiao et al. fabricated highly catalytic, low-resistance Pt flexible counter electrodes with 70% transmittance by vacuum thermal decomposition of H_2PtCl_6 -containing precursors at 100°C , achieving cell efficiencies comparable to FTO glass-based cells under equivalent conditions. Ma Tingli's group synthesized Pt ink at room temperature by reducing H_2PtCl_6 with NaBH_4 and prepared transparent counter electrodes on flexible ITO-PEN substrates by dip-coating at 130°C , achieving a cell efficiency of 5.18% under sunlight using TiO_2 nanocrystals as photoanodes. However, research on simplifying the preparation process while maintaining cell efficiency remains scarce.

In this work, aqueous solutions of $\text{H}_2\text{PtCl}_6 \cdot 6\text{H}_2\text{O}$ with specific mass fractions were used as precursor solutions. After adding appropriate binders, Pt counter electrodes were prepared on FTO substrates by spin-coating combined with annealing-induced thermal decomposition of $\text{H}_2\text{PtCl}_6 \cdot 6\text{H}_2\text{O}$. Based on investigating the photovoltaic performance of DSSCs assembled with counter electrodes prepared under different spin coating-annealing cycles, the Pt concentration in the precursor solution was further optimized, and a one-step drop coating-annealing process was employed to prepare Pt counter electrodes with excellent photoelectric conversion performance.

1.1 Preparation of Pt/FTO Counter Electrodes

Preparation of reaction slurry: Aqueous solution containing 5 g/L $\text{H}_2\text{PtCl}_6 \cdot 6\text{H}_2\text{O}$ and 0.12 g/L ethyl cellulose was mixed with terpineol at a volume ratio of 10:3. OP emulsifier was then added at a ratio of 1 g per 2 mL of mixture, followed by mixing and ultrasonication at room temperature to prepare the reaction slurry. FTO conductive substrates were ultrasonically cleaned sequentially with deionized water, acetone, ethanol, and deionized water for 10 minutes each, then dried with a hair dryer. The reaction solution was coated onto the clean FTO conductive surface using a KW-4A spin coater at low speed (800 rpm) and high

speed (1300 rpm) to form a film, which was then annealed at 450°C for 15 minutes. The spin coating and annealing process was repeated with controlled cycles to obtain counter electrode samples with different Pt loadings.

For one-step prepared Pt counter electrodes, the concentration of $\text{H}_2\text{PtCl}_6 \cdot 6\text{H}_2\text{O}$ aqueous solution was increased fivefold based on the optimized Pt loading. The solution was directly drop-cast onto the FTO substrate and annealed at 450°C for 15 minutes.

1.2 Photoanode Preparation and DSSC Assembly

The photoanode consisted of TiO_2 nanotube arrays prepared in our laboratory. The preparation, peeling, and cell assembly procedures followed those described in references [13, 14]. Briefly, TiO_2 nanotube arrays were fabricated by electrochemical anodic oxidation. After 18 h of anodization, the TiO_2 nanotube arrays were peeled off using 30% hydrogen peroxide, cleaned, and adhered to FTO glass using homemade TiO_2 colloid, followed by annealing at 500°C for 3 h to form crystalline TiO_2 nanotube arrays. The TiO_2 nanotube array/FTO photoanodes were then treated in 0.04 mol/L TiCl_4 aqueous solution for 30 minutes and annealed at 500°C for 1 h. Subsequently, the photoanodes were immersed in 3×10^{-4} mol/L N719 dye solution (with acetonitrile and tert-butanol as solvents at 1:1 volume ratio) for 24 h. The prepared TiO_2 nanotube array/FTO photoanodes were assembled with the counter electrodes into a sandwich structure, and electrolyte was injected to complete the DSSC assembly. The electrolyte consisted of 0.05 mol/L LiI, 0.05 mol/L I_2 , 0.6 mol/L PMII (1-butyl-1-methylimidazolium iodide), and 0.5 mol/L 4-tert-butylpyridine (with acetonitrile and valeronitrile as solvents at 85:15 volume ratio).

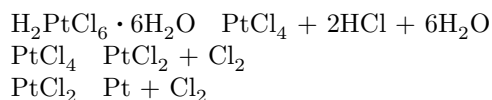
1.3 Sample Characterization

The crystalline properties and microstructure of samples were analyzed using a BRUKER D8 X-ray diffractometer (XRD) and a JSM-7100 scanning electron microscope (SEM). Optical properties of Pt counter electrodes were measured with a UV-3600 UV-Vis-NIR spectrophotometer. Photovoltaic performance of assembled cells was tested using a Newport Oriel solar cell I-V characterization system. For Pt counter electrodes prepared by subsequent drop-coating, the film thickness on FTO substrates might be non-uniform; therefore, multiple measurement results were averaged to reduce error in evaluating Pt loading. The Pt loading on FTO substrates was assessed by measuring the mass difference of conductive substrates before and after experiments using a high-precision analytical balance.

2.1 Structure and Morphology of Pt/FTO Electrodes

Pt counter electrodes were prepared by high-temperature treatment of aqueous $\text{H}_2\text{PtCl}_6 \cdot 6\text{H}_2\text{O}$ solutions. $\text{H}_2\text{PtCl}_6 \cdot 6\text{H}_2\text{O}$ is a water-soluble compound that

partially decomposes at 110°C in humid air and begins forming metallic Pt at 150°C. The reaction equations are as follows:



All three reactions are reversible and proceed forward at high temperatures to generate Pt particles. Figure 1 [Figure 1: see original paper] shows typical XRD patterns of the prepared Pt/FTO counter electrodes. Since single spin-coating produces very thin films with minimal Pt loading, making Pt peaks less distinct compared to the FTO substrate, a sample prepared by nine spin-coating cycles was used for XRD measurement. In addition to characteristic FTO peaks, diffraction peaks corresponding to face-centered cubic Pt(111), (200), and (220) appear successively in the scanning range, confirming successful Pt generation through thermal decomposition of $\text{H}_2\text{PtCl}_6 \cdot 6\text{H}_2\text{O}$. The relatively large full width at half maximum (FWHM) of Pt diffraction peaks indicates small crystallite sizes in the Pt particle films prepared by this method. The crystallite size was estimated using the Scherrer equation:

$$D = \frac{k\lambda}{\beta \cos \theta}$$

where D is the crystallite diameter, k is the shape factor, β is the FWHM of the diffraction peak, λ is the incident X-ray wavelength, and θ is the diffraction angle. A spherical particle shape factor of $k = 0.89$ was used. The calculated crystallite diameter D from the (111) diffraction peak is approximately 25.6 nm, which is consistent with particle sizes measured in subsequent SEM observations. This demonstrates that spin-coating $\text{H}_2\text{PtCl}_6 \cdot 6\text{H}_2\text{O}$ solution followed by short annealing at 450°C successfully produces Pt counter electrodes with small Pt particle sizes. Smaller particles provide larger specific surface area and higher catalytic activity, which is more beneficial for enhancing cell performance.

The Pt loading on FTO substrates was evaluated by measuring the mass difference before and after processing using a high-precision analytical balance. The results show that Pt/FTO counter electrodes prepared by thermal decomposition have a Pt loading of approximately 28.57 g/cm² per spin-coating cycle, with each cycle showing fairly consistent Pt loading increases (deviation < 7%). Since some organic materials may not be completely removed during annealing and trace impurities from the atmosphere may be introduced, the estimated Pt loading is likely higher than the actual Pt loading on the FTO substrate.

Figure 2 [Figure 2: see original paper] presents SEM surface morphologies of clean FTO conductive substrates and Pt/FTO counter electrode samples prepared by different numbers of spin coating-annealing cycles. Figure 2a shows the SEM morphology of pure FTO substrate, where most particles have irregular shapes with a broad size distribution of 30-230 nm. Figure 2b corresponds to a Pt/FTO sample after one spin coating-annealing cycle, where the original

FTO substrate is covered by a film composed of small particles approximately 15 nm in diameter. These particles aggregate irregularly with gaps between aggregates, and the boundaries of aggregates closely follow the morphology of FTO substrate grain boundaries. Due to the small thickness of the single spin-coated sample, Pt reduction and Cl₂ gas volatilization occur during annealing. While Pt particles cover the surfaces of FTO substrate grains relatively uniformly, uniform coverage is difficult to achieve at grain boundaries, resulting in the morphology shown in Figure 2b. As the cycle number increases to three, Pt particles continue to accumulate (Figure 2c), making it difficult to observe clear boundaries of Pt aggregates on the substrate, though some gaps remain visible. Further increasing to five cycles (Figure 2d) results in nearly complete substrate coverage with clearly observable, contrast-bright spherical Pt particles approximately 20 nm in diameter and uniform in size. At seven cycles, increased Pt loading leads to slightly larger Pt particle diameters with an average size of about 32 nm (Figure 2e), and some neighboring particles show connection, which may contribute to the observed particle size increase in SEM. At nine cycles, Pt particle agglomeration becomes evident with blurred particle boundaries (Figure 2f). This occurs because increased spin-coating cycles introduce more reaction solution, and the binder in the solution cannot be completely removed during annealing, leading to Pt particle agglomeration. Such agglomeration may hinder rapid electron transport from the external circuit when assembled into cells, thereby affecting cell efficiency.

2.2 Photovoltaic Performance of DSSCs with Pt/FTO Counter Electrodes

Figure 3 [Figure 3: see original paper] shows the transmittance of Pt/FTO counter electrodes as a function of spin coating cycles. The transmittance is high (>50%) across the 400-800 nm wavelength range, covering nearly the entire visible spectrum. Since N719 dye has optimal light absorption at 515 nm, this wavelength was used as a reference point for transmittance evaluation. As spin coating cycles increase, the transmittance of Pt/FTO counter electrodes decreases from 80% for one cycle to 73% (three cycles), 70% (five cycles), 66% (seven cycles), and finally 59% for nine cycles. This is attributed to increased Pt particle deposition and film thickness on the FTO substrate. In DSSCs operating in back-illumination mode (light entering through the counter electrode), high-transmittance counter electrodes are typically used to minimize optical losses. The high optical transmittance of Pt/FTO counter electrodes prepared by thermal decomposition makes them highly suitable for solar cells that can only operate in back-illumination mode.

To evaluate the performance of thermally prepared Pt counter electrodes in DSSCs, TiO₂ nanotube arrays prepared by anodic oxidation were used as photoanodes and assembled with electrolyte and counter electrodes into sandwich-structured DSSCs. Their photovoltaic performance was tested under front-illumination mode. Figure 4 [Figure 4: see original paper] shows J-V curves

of DSSCs assembled with different counter electrodes, with corresponding cell performance parameters listed in Table 1 .

For cells using thermally prepared counter electrodes, the open-circuit voltage (V_{oc}) shows little variation with increasing spin coating cycles, while the short-circuit current density (J_{sc}) increases from $12.17 \text{ mA} \cdot \text{cm}^{-2}$ for one cycle to a maximum of $15.55 \text{ mA} \cdot \text{cm}^{-2}$ for five cycles. Further increasing spin coating cycles leads to gradual decreases in J_{sc} to $14.88 \text{ mA} \cdot \text{cm}^{-2}$ (seven cycles) and $12.34 \text{ mA} \cdot \text{cm}^{-2}$ (nine cycles). The fill factor (FF) and efficiency (η) follow similar trends, increasing from 43.75% (FF) and 4.10% (η) for one cycle to maximum values of 57.52% (FF) and 6.78% (η) for five cycles, then decreasing with further cycles. At low cycle numbers, SEM results show incomplete coverage of the FTO substrate by Pt particles, preventing rapid electron extraction at the counter electrode and causing more severe carrier recombination, which results in lower FF and J_{sc} and consequently lower efficiency. As spin coating cycles increase, the Pt particle film becomes more complete, enabling rapid electron extraction while preventing direct contact between electrolyte/dye and FTO, thereby suppressing carrier recombination and enhancing catalytic reduction of the I^-/I_3^- redox couple. Consequently, five-cycle samples achieve maximum FF, J_{sc} , and efficiency. However, when cycles increase beyond seven, some organic impurities in the counter electrode cannot be completely removed during annealing. Hauch et al. found that impurities in counter electrodes reduce Pt catalytic activity and hinder electron transfer between the Pt electrode and electrolyte, leading to decreased FF, J_{sc} , and efficiency as observed in cells with seven and nine-cycle counter electrodes. Additionally, under front-illumination conditions, an optimal counter electrode thickness enables multiple reflections of incident light within the photoanode and dye, improving light utilization, enhancing light harvesting, promoting photoelectron generation, and increasing electron injection efficiency (positively correlated with J_{sc}) and cell efficiency. However, excessively thick Pt particle films introduce more particle-particle interfaces, lengthening the electron transport path to the I_3^- acceptor and increasing electron recombination probability, which contributes to the observed initial increase and subsequent decrease in J_{sc} .

For comparison with conventional magnetron sputtered Pt counter electrodes, cells were assembled using the same photoanodes and optimized sputtering parameters (30 s sputtering time, 125 nm film thickness, corresponding to Pt loading of approximately $268.14 \text{ g}/\text{cm}^2$ and particle size of about 80 nm). The J-V curve and photovoltaic parameters are also presented in Figure 4 and Table 1. The results show that under optimal conditions (five spin coating-annealing cycles), thermally prepared Pt counter electrodes achieve slightly higher cell efficiency (6.78%) than magnetron sputtered Pt counter electrodes (6.62%). Compared to sputtered Pt counter electrodes, thermally prepared ones exhibit significantly higher V_{oc} but lower FF. The higher V_{oc} may be attributed to: (1) smaller Pt particles in thermally prepared counter electrodes providing more complete contact and higher catalytic activity, facilitating carrier conduction and collection in the cell and promoting rapid I_3^- reduction, thereby enhancing

Voc; (2) thinner thermally prepared Pt counter electrodes resulting in shorter carrier transport paths, which helps suppress carrier recombination with dye and electrolyte and also benefits Voc. The higher FF of DSSCs with magnetron sputtered Pt counter electrodes may result from better film flatness and denser morphology. Additionally, organic impurities in thermally prepared samples may also affect FF. Overall, thermally prepared Pt counter electrodes with five spin coating cycles outperform conventional magnetron sputtered Pt counter electrodes, with lower Pt consumption and simpler, less energy-intensive fabrication processes.

2.3 One-step Preparation of Pt/FTO Counter Electrodes and Their Structure and Performance

Based on the above discussion, thermal decomposition of $\text{H}_2\text{PtCl}_6 \cdot 6\text{H}_2\text{O}$ aqueous solution with appropriate spin coating-annealing cycles can produce Pt counter electrodes with low Pt loading, high transmittance, and high catalytic activity, achieving superior DSSC efficiency compared to conventional magnetron sputtered Pt counter electrodes. Under optimal cell efficiency conditions, the Pt loading is 142.85 g/cm^2 , significantly reducing precious metal consumption. To further simplify the fabrication process, we aimed to prepare Pt counter electrodes with similar performance through a one-step process. Therefore, the concentrations of $\text{H}_2\text{PtCl}_6 \cdot 6\text{H}_2\text{O}$ and ethyl cellulose in the reaction solution were increased fivefold. To minimize solution loss during spin-coating and maximize Pt utilization, 40 L of the chloroplatinic acid solution was directly drop-cast onto a 4 cm^2 FTO substrate, spread uniformly with a toothpick, allowed to stand for a period, and then annealed at 450°C for 15 minutes to prepare Pt/FTO counter electrodes by a one-step method.

Figure 5a [Figure 5: see original paper] shows the XRD pattern of the Pt/FTO counter electrode. In addition to FTO substrate peaks, Pt(111), (200), and (220) diffraction peaks are clearly observed, confirming that one-step annealing treatment of $\text{H}_2\text{PtCl}_6 \cdot 6\text{H}_2\text{O}$ solution effectively reduces Pt ions to form Pt counter electrodes. Figure 5b shows the transmittance of the Pt/FTO counter electrode, which reaches 72%—slightly higher than that of the five-cycle spin coating-annealed counter electrode that achieved optimal efficiency—indicating that the one-step prepared electrode may be slightly thinner. The mass difference of FTO substrates before and after processing was measured using a high-precision analytical balance, yielding a Pt loading of approximately 124.28 g/cm^2 for the one-step prepared Pt/FTO counter electrode, slightly lower than that of the five-cycle sample, consistent with the transmittance results. This may be because the drop-cast solution contained less terpineol than the total amount used in five spin-coating cycles, resulting in less organic residue after annealing and consequently lower measured Pt loading. In fact, ignoring solution loss during preparation and assuming complete reduction of Pt from $\text{H}_2\text{PtCl}_6 \cdot 6\text{H}_2\text{O}$ on the FTO substrate, the Pt content can be roughly estimated from the solution volume and concentration as 72.16 g/cm^2 , which is about 58%

of the mass difference measured before and after substrate processing. This indicates that the substrate still contains considerable residual organics or partially unreduced PtCl_2 and PtCl_4 . The Pt consumption is only 27% of that for magnetron sputtered Pt counter electrodes. Figure 5c shows the J-V curve of DSSCs assembled with this Pt counter electrode and the same TiO_2 nanotube photoanode. The short-circuit current ($J_{sc} = 15.60 \text{ mA} \cdot \text{cm}^{-2}$) and open-circuit voltage ($V_{oc} = 0.76 \text{ V}$) are essentially equivalent to those of DSSCs assembled with five-cycle spin coating-annealed counter electrodes. The fill factor (FF = 58.52%) and efficiency ($\eta = 6.92\%$) of cells with one-step prepared counter electrodes are slightly higher than those of the five-cycle sample, possibly due to cell-to-cell variations. Figure 5d shows the SEM image of the one-step prepared Pt/FTO counter electrode, revealing nearly complete substrate coverage by uniform Pt particles approximately 20 nm in diameter, consistent with the five-cycle spin-coated electrode. Despite some agglomeration due to organic residue during annealing, the particle boundaries remain clear, enabling good photovoltaic performance in assembled cells.

3 Conclusion

Thermal decomposition of $\text{H}_2\text{PtCl}_6 \cdot 6\text{H}_2\text{O}$ aqueous solution through cyclic spin coating-annealing can produce Pt counter electrodes with low Pt loading, high transmittance, high catalytic activity, and high DSSC energy conversion efficiency. Under five spin coating-annealing cycles, DSSCs based on TiO_2 nanotube array photoanodes achieved an efficiency of 6.78%, surpassing that of cells with conventional magnetron sputtered Pt counter electrodes (6.62%). Based on the mass difference before and after processing, the Pt loading is 142.85 g/cm^2 , significantly reducing precious metal consumption. To further simplify the process, the $\text{H}_2\text{PtCl}_6 \cdot 6\text{H}_2\text{O}$ concentration was increased fivefold, and a one-step drop coating-annealing process was used to prepare Pt counter electrodes with similar performance. The resulting electrodes exhibited uniform particle coverage, consistent particle size ($\sim 20 \text{ nm}$), 72% transmittance, and Pt loading of only 27% of conventional magnetron sputtered counter electrodes, while achieving a DSSC photoelectric conversion efficiency of 6.92%. The drop coating-annealing method for preparing Pt counter electrodes not only greatly simplifies the fabrication process and reduces energy consumption but also minimizes precious metal consumption while improving assembled cell performance.

References

1. B. O' Regan, M. Grätzel, Principle of dye sensitized solar cell, *Nature*, 353, 737(1991)
2. M. Grätzel, Photoelectrochemical cells, *Nature*, 414, 338(2001)
3. N. Papageorgiou, Counter-electrode function in nanocrystalline photoelectrochemical cell configurations, *Coor. Chem. Rev.*, 248, 1421(2004)

4. W. J. Lee, E. Ramasamy, D. Y. Lee, J. S. Song, Performance variation of carbon counter electrode based dye-sensitized solar cell, *Sol. Energy Mater & Sol. Cells*, 92, 814(2008)
5. J. Y. Lin, Y. T. Lin, Electroless platinum counter electrodes with Pt-activated self-assembled monolayer on transparent conducting oxide, *Surf. Coat. Tech*, 206, 4672(2012)
6. Y. D. Wang, M. X. Wu, X. Lin, Z. C. Shi, A. Hagfeldt, T. L. Ma, Several highly efficient catalysts for Pt-free and FTO-free counter electrodes of dye-sensitized solar cells, *J. Mater. Chem.*, 22, 4009(2012)
7. X. M. Fang, T. L. Ma, G. Q. Guan, M. Akiyama, T. Kida, E. Abe, Effect of the thickness of the Pt film coated on a counter electrode on the performance of a dye-sensitized solar cell, *J. Electroanal. Chem.*, 570, 257(2004)
8. J. Y. Lin, Y. T. Lin, Electroless platinum counter electrodes with Pt-activated self-assembled monolayer on transparent conducting oxide, *Surf. Coat. Tech*, 206, 4672(2012)
9. X. L. He, M. Liu, G.J.Yang, S. Q. Fan, C. J. Li, Correlation between microstructure and property of electroless deposited Pt counter electrodes on plastic substrate for dye-sensitized solar cells, *Appl. Surf. Sci.*, 258, 1377(2011)
10. (Reference incomplete in original)
11. Y. M. Xiao, J. H. Wu, C. X. Cheng, Y. Chen, G. T. Yue, J. M. Lin, M. L. Huang, L. Q. Fang, Z. Lan, Low temperature fabrication of high performance and transparent Pt counter electrodes for use in flexible dye-sensitized solar cells, *Chin. Sci. Bull.*, 57, 2329(2012)
12. Y. D. Wang, C. Y. Zhao, D. Qin, M. X. Wu, W. Liu, T. L. Ma, Transparent flexible Pt counter electrodes for high performance dye-sensitized solar cells, *J. Mater. Chem.*, 22, 22155(2012)
13. J. Zhang, S. Q. Li, H. Ding, Q. T. Li, B. Y. Wang, X. N. Wang, H. Wang, Transfer and assembly of large area TiO₂ nanotube arrays onto conductive glass for dye sensitized solar cells, *J. Power Source*, 247, 807(2014)
14. J. Zhang, Q. T. Li, S. Q. Li, Y. Wang, C. Ye, P. Ruterana, H. Wang, An efficient photoanode consisting of TiO₂ nanoparticle-filled TiO₂ nanotube arrays for dye sensitized solar cells, *J. Power Source*, 268, 941(2014)
15. A. Monshi, M. R. Foroughi, M. R. Monshi, Modified scherrer equation to estimate more accurately nano-crystallite size using XRD, *World J. Nano Sci. Eng.*, 2, 154(2012)
16. Saito Y, Kubo W, Kitamura T, Wada Y, Yanagida S, I⁻/I₃⁻ redox reaction behavior on poly(3,4-ethylenedioxythiophene) counter electrode

- in dye-sensitized solar cells, *J. Photochem Photobiol A: Chem.*, 164, 153(2004)
17. (Reference incomplete in original)
 18. D. S. Zhang, T. Yoshida, K. Furuta, H. J. Minoura, Hydrothermal preparation of porous nanocrystalline TiO_2 electrodes for flexible solar cells, *Photochem Photobiol A: Chem.*, 164, 159(2004)
 19. K. Imoto, K. Takahashi, T. Yamaguchi, T. Komura, J. Nakamura, K. Murata, High-performance carbon counter electrode for dye-sensitized solar cells, *Sol. Energy Mater. Sol. Cells*, 79, 459(2003)
 20. M. Paulose, O. K. Varghese, G. K. Mor, C. A. Grimes, Unprecedented ultra-high hydrogen gas sensitivity in undoped titania nanotubes, *Nanotechnol.*, 17, 4285(2006)
 21. A. Hauch, A. Georg, Diffusion in the electrolyte and charge-transfer reaction at the platinum electrode in dye-sensitized solar cells, *Electrochim. Acta*, 46, 3457(2001)

Note: Figure translations are in progress. See original paper for figures.

Source: ChinaXiv – Machine translation. Verify with original.